Lab on a Chip

A Transparent Low Intensity Pulsed Ultrasound (LIPUS) Chip for High-throughput Cell Stimulation

Journal:	*Lab on a Chip*
Manuscript ID	LC-COM-07-2021-000667.R1
Article Type:	Communication
Date Submitted by the Author:	17-Oct-2021
Complete List of Authors:	Chen, Haoyang; Penn State University Park, Biomedical Engineering Zhu, Ninghao; Penn State, Biomedical Engineering Osman, Mohamed; Penn State University Park, Biomedical Engineering Biskowitz, Ryan; Penn State University Park, Biomedical Engineering Liu, Jinyun; Penn State University Park, Biomedical Engineering Khandare, Shubham; Penn State University Park, Biomedical Engineering Butler, Peter; Penn State University Park, Biomedical Engineering Wong, Pak; Penn State University Park, Biomedical Engineering; Penn State University Park, Mechanical Engineering Kothapalli, Sri-Rajasekhar; Penn State University Park, Biomedical Engineering; Penn State Cancer Institute

COMMUNICATION

A Transparent Low Intensity Pulsed Ultrasound (LIPUS) Chip for High-throughput Cell Stimulation

Received 00th January 20xx,
Accepted 00th January 20xx

DOI: 10.1039/x0xx00000x

Haoyang Chen[a], Ninghao Zhu[a], Mohamed Osman[a], Ryan Biskowitz[a], Jinyun Liu[a], Shubham Khandare[a], Peter Butler[a], Pak Kin Wong[a,b] and Sri-Rajasekhar Kothapalli[a,c]

We report an on-chip platform for low-intensity pulsed ultrasound (LIPUS) stimulation of cells directly cultured on a biocompatible surface of a transparent ultrasound transducer (TUT) fabricated using lithium niobate. The high light transmittance (> 80%) and compact size (3 mm × 3 mm × 2 mm) of TUTs allow for easy integration with powerful optical microscopy techniques with no additional acoustic coupling and risk for contamination. TUTs were excited with varying acoustic excitation parameters (voltage amplitude and duty cycle) and resulting live cell calcium signaling was simultaneously imaged using time-lapse confocal microscopy and the temperature change was measured by a thermocouple. Quantitative single-cell fluorescence analysis revealed dynamic calcium signaling responses and together with temperature measurements revealed optimal stimulation conditions for non-thermal and thermal effects. The fluorescence change profile was distinct from the recorded temperature change (< 1 degree Celsius) profile under LIPUS treatment conditions. Cell dead assay results confirmed cells remain viable after LIPUS treatment. The TUT platform enables controllable, safe, high-throughput, and uniform mechanical stimulation of all plated cells. The on-chip LIPUS using TUTs has the potential to attract several *in vitro* and *in vivo* biomedical applications such as controlling stem cell differentiation and proliferation, studying biomechanical properties of different cancer cells, and gaining fundamental insights into mechanotransduction pathways when integrated with state-of-the-art high speed and high-resolution microscopy techniques.

Introduction

Low intensity pulsed ultrasound (LIPUS) stimulation uses non-invasive and non-ionizing delivery of mechanical energies to stimulate biological subjects of different scales, from cells in culture to whole organs in living animals and humans. Therefore, LIPUS stimulation has emerged as a precious biomedical tool for several preclinical studies and clinical applications, including neuromodulation (1), pain alleviation (2), inflammation mediation (3), and tissue and bone healing (4). In particular, ultrasound stimulation of various types of cells in culture have been actively investigated by various groups because mechanical forces are known to play a key role in modulating various cell functions such as controlling stem cell differentiation and proliferation (7), cancer cell apoptosis (5), cell migration (6), delivering genes and molecules into cells for personalized immunotherapy (7, 8), and extracellular matrix remodelling by activating mechanotransduction pathways followed by gene expressions (9, 10). Studying the effect of LIPUS on cell morphology, cell-to-cell communication, and related downstream signaling pathways facilitate the understanding of the LIPUS-induced mechanotransduction effects at cellular and subcellular levels.

Although recent progress has identified that cell Ca^{2+} signaling induced by non-thermal effects were involved in LIPUS cell stimulations (11-13), the underlying molecular mechanisms and mechanotransduction signaling pathways are not yet fully understood, often leading to confounding results. This is likely due to variations between experiments that lack full control in reproducibility and inconsistent acoustic stimulation parameters. Therefore, a reliable LIPUS platform is needed for simultaneous and uniform stimulation of all the cells in culture, defined as high-throughput stimulation in this study. Currently, two setups are used for active ultrasound stimulation of cells in culture. In one setup a focused ultrasound transducer directs ultrasound waves to cells in a cultured dish, placed at the focal distance from the transducer, from an angle to allow imaging of cell calcium signals using an upright microscope (14, 15). This configuration requires the transducer, cell culturing dish, and/or microscopic objective to be submerged inside a water tank, leading to non-sterile working conditions. The cells in the focal spot of the transducer are stimulated first and this generates a calcium gradient, and subsequent calcium waves propagate from the focal spot to the surrounding regions and evoke calcium signaling responses from the cells in those regions. Therefore, this setup is not optimal for long-term or repeated stimulation studies like wound healing and for applications that require a uniform and synchronized stimulation of all cells. In the second setup, an ultrasound

[a] *Department of Biomedical Engineering, The Pennsylvania State University, University Park, PA 16802, USA.*
[b] *Department of Mechanical Engineering, The Pennsylvania State University, University Park, PA 16802, USA.*
[c] *Penn State Cancer Institute, The Pennsylvania State University, Hershey, PA 17033, USA.*
Electronic Supplementary Information (ESI) available: [details of any supplementary information available should be included here]. See DOI: 10.1039/x0xx00000x

transducer is directly coupled to the bottom of a petri dish containing cells in culture (16-18). The advantage of this setup is it requires minimal acoustic coupling and reduces the possibility of cell contamination. However, because ultrasound waves must first pass through the bottom dish plate, and thereby undergo distortion before stimulating the cells, it is difficult to achieve high-throughput and uniform stimulation of all cells using this approach. This technique is also limited to low-frequency (~ 1 to 2 MHz) to partially offset the acoustic losses through the dish plate. Moreover, conventional ultrasound transducers are opaque to light and thus making it difficult to integrate this setup with high-resolution optical microscopy to observe cell behaviours during the stimulation with bright and fluorescence field at the same time to display a wide range of bioinformation.

Here, we report an on-chip *in vitro* LIPUS cell stimulation study platform using a transparent ultrasound transducer (TUT) made of a transparent lithium niobate ($LiNbO_3$) piezoelectric material. Fig. 1a shows the schematic of the experimental setup. The TUT platform overcomes all the above-mentioned hurdles by directly plating the cells on top of the parylene-coated biocompatible TUT surface. Thereby this platform eliminates the need for additional acoustic coupling, such as submerging the transducer and cell culture medium in a water tank, and associated risk for cell contamination. The superior transparency (> 80%) (19) and compact dimensions (3 mm x 3 mm x 2 mm) of the TUT allow easy integration with conventional optical microscopy for simultaneous bright field and fluorescence imaging of the induced biological effects inside cells during stimulation. By plating bladder cancer cells on the TUT surface and systematically exciting the TUTs with various stimulation parameters (voltage amplitude, pulse duration, duty cycle) using the timing diagram shown in Fig. 1b,

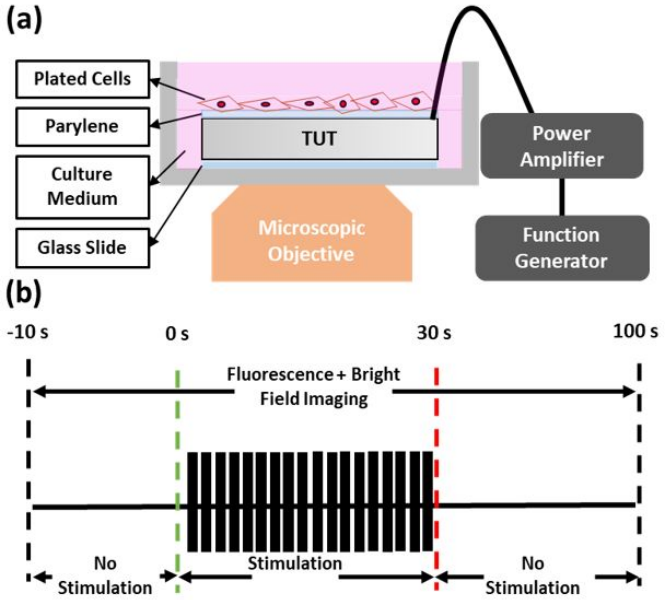

Fig. 1: The reported setup for low intensity pulsed ultrasound (LIPUS) stimulation experiments: **(a)** experimental setup. TUT – transparent ultrasound transducer; **(b)** The timing diagram (not to scale) of a general stimulation setup. Green line indicates the time when the stimulation is turned on, and red line indicates the time when the stimulation is turned off.

we studied optimal conditions for inducing non-thermal (LIPUS) and thermal effects. Our results show that all the cells were uniformly stimulated in a simultaneous manner and the temperature change can be controlled with stimulation parameters. The stimulation platform is safe and biocompatible; Cell dead assay staining 48 hours after the stimulation revealed a cell viability of > 93%, making the platform suitable for short-term and long-term stimulation scenarios.

Results and Discussion

TUT transparency test

We first analyzed the transparency of the fabricated TUT and the morphology of cells plated on top of the TUT surface. The bright field images of the cells from the 10× air coupled objective lens are shown in Fig. 2. Fig. 2a shows the live cells plated on top of the TUT and Fig. 2b shows a zoomed-in picture of cells shown in Fig. 2a. The cell boundaries can be clearly resolved with minimal light aberration in both the images. These results show the feasibility of high-resolution imaging of cells through the TUT. The current TUT thickness (2 mm) restricts a higher magnification objective lens (e.g., 63x) from being employed because of the limited working distance. However, the brass housing height of the TUT and piezoelectric material thickness can be reduced for applications that require greater magnification and higher spatial resolution.

Acoustic field and pressure output characterization of TUT

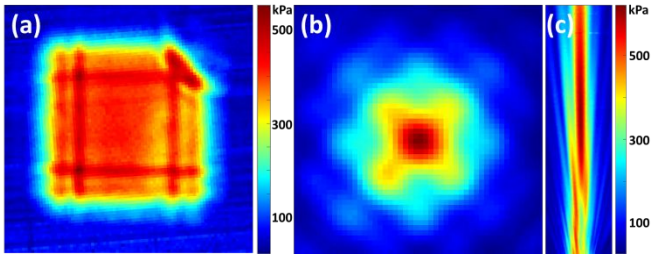

Fig. 3: Hydrophone-measured acoustic pressure fields for the transparent ultrasound transducers (TUT) **(a)** near field at 1 mm away from the transducer surface, and **(b)** far field X-Y plane at 20 mm, which is the natural focus of the TUT. **(c)** X-Z plane from near field to far field. Scale bars are displayed at the top right of each image in white and represent 1 mm.

Different than surface acoustic wave (SAW) devices, LIPUS devices mainly utilize longitudinal wave for inducing bioeffects (20, 21). Therefore, a 36° rotated Y-cut transparent $LiNbO_3$ was used to build the TUT, as its mechanical vibration is predominantly in the quasi-longitudinal mode along the direction of the propagation of the wave. This is confirmed by finite element analysis modelling using COMSOL (see Materials and Methods section and Supplementary Video S1). To check the uniformity of the pressure distribution, we characterized the pressure output from the TUTs in the near and far field regions using a scanning hydrophone, and the procedures are outlined in the Materials and Methods section. Fig. 3 presents the calibrated pressure output results. Fig. 3a shows the hydrophone measured X-Y plane pressure map for the TUT at the near field (1 mm away from the transducer surface) while the transducer was excited by 5 V peak-to-peak (Vpp) at 13 MHz with a 20 dB gain power amplifier. The absolute pressure was measured to be 0.397 MPa ± 0.037 MPa across the surface (Fig. 3a). This shows the near field pressure across the transducer surface is uniform and demonstrates the feasibility of uniform stimulation of plated cells. Fig. 3b shows the far-field X-Y plane pressure map recorded by hydrophone at Z = 20 mm away from the TUT surface, which is the natural focus of this planar TUT. The full width half maxima (FWHM) of the beam profile at the focus was found to be 190 µm. The peak pressure at the focal point was measured to be 0.62 MPa. Fig. 3c shows the X-Z plane pressure map of the TUT from the near field to the far field.

LIPUS cell stimulation

Next, we validated the TUT capabilities for LIPUS stimulation of the plated cells. The bladder cancer cells were stimulated with 3 Vpp amplitude (with 20 dB gain power amplifier), 500 Hz pulse repetition frequency (PRF), and 25% duty cycle for 30 seconds duration. The corresponding spatial peak temporal average intensity (I_{SPTA}) value was calculated to be 51.3 mW/cm^2, and the spatial peak pulse average intensity (I_{SPPA}) value was calculated to be 0.205 W/cm^2 with a mechanical index (MI) of 0.003. These values are below FDA safety limits for diagnostic ultrasound (22) as well as within the LIPUS stimulation thresholds. The intracellular calcium variations covering pre-stimulation, stimulation, and post-stimulation time periods – are recorded by time-lapse confocal microscopy (Supplementary Video S2) in both bright and fluorescence modes at 1 frame per second. Fig. 4a shows six example frames at different timepoints of the video. The single-cell fluorescence was quantified (see Methods and Materials section) for each of the acquired fluorescence image frame. Fig. 4b shows the single-cell analysis spectrogram, where the Y-axis represents the relative changes in calcium fluorescence for each cell against time (X-axis). During the 10-second baseline (before stimulation), the calcium fluorescence did not have observable fluctuation (Figs. 4a-b). When the stimulation was turned on at t = 0 seconds, the intracellular calcium fluorescence kept

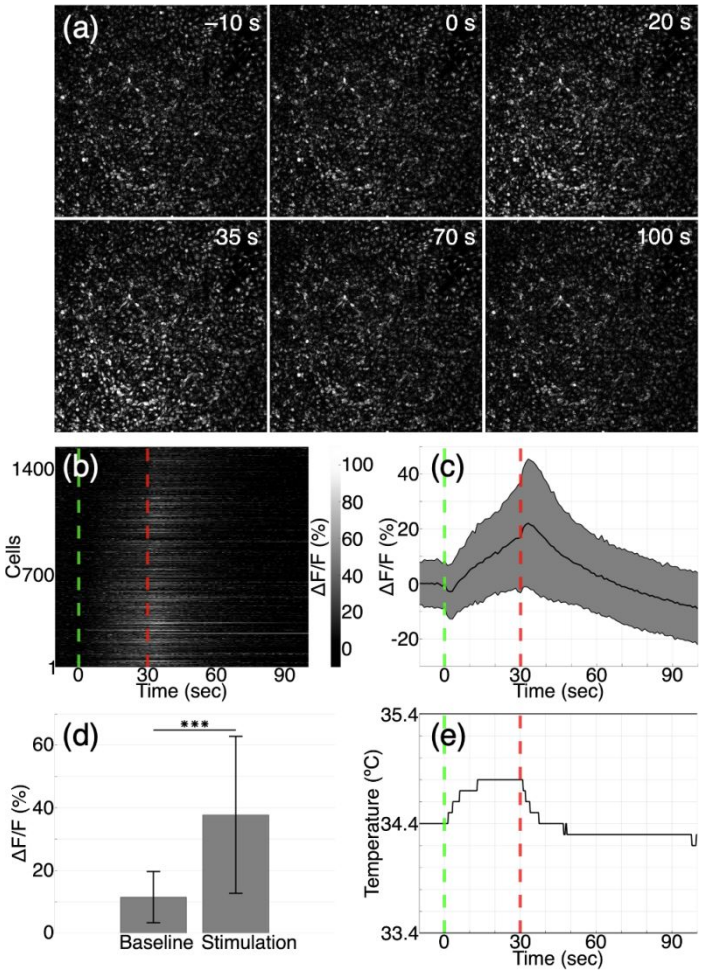

Fig. 4: Low intensity pulsed ultrasound on-chip cell stimulation results: **(a)** the time-lapsed confocal microscopy images of calcium fluorescence for the plated bladder cancer cells. The ultrasound stimulation was turned on at t = 0 seconds and turned off at t = 30 seconds. **(b)** The single-cell analysis spectrogram, green dashed line indicates the start of stimulation, and red dashed line indicates the end of stimulation. **(c)** Fluorescence relative changes for single cell. The solid line indicates the averaged single cell fluorescence changes, and the grey shading indicates the standard deviations. **(d)** Statistical analysis compared the averaged single-cell baseline fluorescence fluctuation and its maximum fluorescence relative changes. Error bar indicates the +/- standard deviation, and three asterisks indicates the statistical significance ($p < 0.001$). **(e)** The measured temperature change on the surface of the transparent ultrasound transducer. Green dashed line indicates the start of stimulation, and red dashed line indicates the end of stimulation.

increasing during the 30 seconds stimulation period across all plated cells (Figs. 4b-c). Then the stimulation was turned off at t = 30 seconds, and we observed that the calcium fluorescence continued to increase, peaking at around t = ~34 seconds (Figs. 4b-c), with an averaged single-cell peak fluorescence change of 22.06%, then slowly decayed down to their original fluorescence intensity level (Figs. 4a-c). These results show that the trend and relative intensity change for each cell was similar and synchronized for all plated cells. Statistical analysis was then conducted to compare each cell's baseline fluorescence level change (t = -10 seconds to t = 0 second) to their maximum fluorescence level change (see Materials and Methods section). During the baseline period, the fluorescence fluctuations was found to be 11.52% ± 8.15%, while the maximum fluorescence change fluctuation was found to be 37.77% ± 25.01% (Fig. 4d). The change was statistically significant with a p-value < 0.001, indicating the intracellular calcium level was successfully altered with the proposed platform. The fact that the cell morphology and calcium fluorescence intensity did not change appreciably between the pre- and post- stimulation time points (t = 0 seconds and t = 100 seconds (Fig. 4a)), shows that the cell viability is intact after the LIPUS treatment. This was further confirmed using dead assay studies conducted immediately after the stimulation and at 48 hour time point after the stimulation experiments (Supplementary Figs. S1a-b). By conducting the cell segmentation, the live cell ratio was calculated to be 99.87% and 93.02% respectively, which is similar to other works reported literature (23).

LIPUS stimulation effect is often considered as a mixture of thermal and non-thermal (mechanical) effects (24). However, mechanical effect is viewed as the dominant effect when a temperature increase is less than 1° C (25, 26). To investigate whether the intracellular calcium increase is strongly associated with the thermal effect, we measured the temperature increase at the TUT surface using a thermocouple (see Materials and Methods section). Fig. 4e shows that, with a 3 Vpp and 25% duty cycle stimulation parameter, the temperature increase was 0.4 °C (increased from 34.4 °C 34.8 °C), which well below 1 °C, during the 30 second stimulation period. Comparing the intracellular fluorescence change curve (Fig. 4c) and temperature change curve (Fig. 4e), it can be observed that while the temperature change plateaued at around t = 15 seconds, the intracellular calcium level continued increasing during the whole 30 second stimulation period and even a few seconds beyond till t = 34 seconds (stimulation was turned off at t =30 seconds). This distinction between the two curves confirmed, in a way, that the intracellular calcium change was mainly due to the acoustic and mechanical effects from the TUT platform.

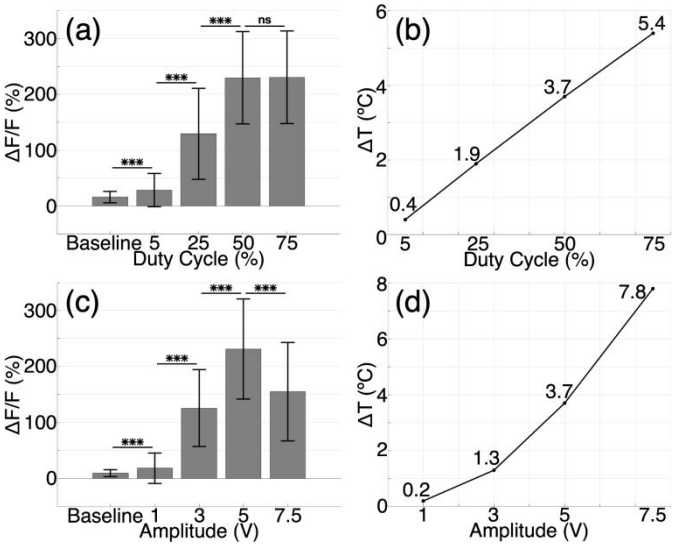

Fig. 5: Stimulation effect with different stimulation parameters: **(a)** The averaged single-cell maximum fluorescence relative changes versus varied stimulation duty cycle for each cell. Error bar indicates the +/- standard deviation, and three asterisks indicates the statistical significance (p < 0.001). ns: not significant. **(b)** The measured maximum temperature change versus varied stimulation duty cycle with a fixed amplitude of 5 Vpp. **(c)** The averaged single-cell maximum fluorescence changes versus varied amplitude LIPUS stimulation. Error bar indicates the +/- standard deviation, and three asterisks indicates the statistical significance (p < 0.001). **(d)** The measured maximum temperature change versus varied stimulation amplitude with a fixed duty cycle of 50%.

Effect of different stimulation parameters

To further study how different stimulation parameters induce non-thermal and thermal effects, here we varied stimulation amplitude and duty cycle and measured corresponding changes in the TUT temperature and intracellular calcium fluorescence. First, we maintained the peak-to-peak voltage of 5 Vpp and power amplifier gain of 20 dB while varying the duty cycle between 5%, 25%, 50%, and 75%. The corresponding I_{SPTA} values are 28.5 mW/cm^2, 142.5 mW/cm^2, 285 mW/cm^2, and 427.5 mW/cm^2 respectively, and the I_{SPPA} value is 0.57 W/cm^2. The resultant peak calcium fluorescence changes averaged across all imaged cells for these duty cycles are shown in Fig. 5 and the associated maximum surface temperature changes are plotted in Fig. 5b. 5% duty cycle induced a fluorescence increase of 28.58% ± 29.91% and a temperature change of 0.4 °C. This temperature change is less than 1 °C while the fluorescence change was still statistically significant compared to the baseline reading of 16.05% ± 10.44%, indicating the intracellular calcium increase was majorly contributed by the non-thermal mechanical forces. 25% duty cycle had a fluorescence increase of 129.40% ± 81.32% and 50% duty cycle stimulation further increased the fluorescence change to 229.48% ± 82.62%. Meanwhile, the surface temperature increased with duty cycle in a linear fashion from 0.4 °C change at 5% duty cycle to 5.4 °C change at 75% duty cycle. Interestingly, although 75% duty cycle had an increased acoustic intensity (I_{SPTA}) and resulted in ~1.7 °C temperature increase from that of the 50% duty cycle excitation, the fluorescence change (230.72% ± 83.06%) was not statistically different than the 50% duty cycle session. This result indicated that the fluorescence increase could be saturated at 50% duty cycle.

Next, we maintained the duty cycle at 50%, stimulation time period of 30 seconds, the gain of the power amplifier at 20 dB and varied the stimulation peak to peak amplitude at 1 V, 3 V, 5 V, and 7.5 V. The corresponding I_{SPTA} values were 11.4 mW/cm^2, 102.6 mW/cm^2, 285 mW/cm^2, 641.25 mW/cm^2, respectively, and corresponding I_{SPPA} values were 0.023 W/cm^2, 0.205

W/cm^2, 0.57 W/cm^2, and 1.28 W/cm^2, respectively. Fig. 5c shows the maximum calcium fluorescence change averaged across all imaged cells versus stimulation amplitude and Fig. 5d plots the associated maximum surface temperature change of the TUT. From 1 Vpp to 5 Vpp, the intracellular calcium fluorescence and temperature increased with increased amplitude. Although 1 Vpp had a relatively small increase of 18.4% fluorescence change and a temperature increase of 0.2 °C, the calcium fluorescence was still statistically significant when compared to the baseline fluorescence fluctuation of 9.77% ± 6.19% (Fig. 5c). 5 Vpp induced the most significant intracellular calcium fluorescence change with an average change of 231.32% ± 89.24% across all imaged cells. However, when the amplitude was further increased to 7.5 Vpp, the maximum surface temperature change increased to 7.8 °C, and the averaged peak intracellular fluorescence change decreased to 155.00%. We hypothesized that this was due to cell death after exposure to rapid temperature change and high acoustic intensity (I_{SPTA} 641.25 mW/cm^2 and I_{SPPA} 1.28 W/cm^2). Subsequent dead assay tests performed one-hour after the 7.5 Vpp, 30 second stimulation, and 50% duty cycle treatment confirmed that live cell ratio was less than 1% (Supplementary Fig. S2).

These results indicated that both the TUT surface temperature and the intracellular fluorescence change of cells plated on the TUT is controllable with acoustic stimulation parameters. Noteworthily, varying duty cycle study (Figs. 5a-b) and varying voltage amplitude study (Fig. 5c-d) both demonstrated the same maximum temperature increase (3.7 °C) and a similar increase (~ 230%) in averaged single-cell calcium fluorescence for a combination of 50% duty cycle and 5 Vpp excitation. While Fig. 3 results demonstrated that 3 Vpp and 25% duty cycle stimulation resulted in mechanical or non-thermal (< 1 °C temperature change) cell stimulation, the 5 Vpp and 50% duty cycle stimulation with a 3.7 °C temperature change induced a combination of non-thermal and thermal effects without affecting the cell viability (90.7% alive tested with dead assay at t = 48 hours, figure not shown). For the 5 Vpp and 50% duty cycle excitation, the cell calcium fluorescence signaling movie is shown in Supplementary Video S3, and single-cell fluorescence analysis results are shown in Supplementary Fig. S3. All these results demonstrate that the TUT stimulation platform is robust and reproducible in terms of inducing both non-thermal and thermal effects. The proposed *in vitro* TUT platform can also be extended for applications that need to study the ultrasound stimulation induced thermal effects, such as selective cancer cell destruction (27, 28) and bone growth (29, 30).

Transient ultrasound stimulation

As discussed above, both the mechanical and thermal effects are rapid and possible with the proposed TUT platform. Because cells were directly contacting the transducer surface, we hypothesized that a transient (< 1 second) stimulation should be sufficient to induce a temporary intracellular calcium increase. Using the stimulation parameters that safely induced both mechanical and thermal effects (5 Vpp from function generator, 20 dB gain, 50% duty cycle and 500 Hz PRF with an I_{SPTA} of 285 mW/cm^2 and I_{SPPA} of 0.57 W/cm^2), we stimulated the bladder cancer cells for 0.5 seconds, while acquiring both fluorescence and bright field images at 2 frames per second. Similar to the previous stimulation timing diagram – Fig. 1b, we first imaged cells for 10 seconds with no stimulation to provide a baseline reading. The stimulation was turned on at t = 0 seconds for a 0.5 second duration. Interestingly, it was found that 0.5 seconds of ultrasound stimulation did induce a small intracellular calcium increase across all the plated cells (Supplementary Video S4, and Supplementary Fig. S4). The averaged single-cell peak fluorescence change was calculated to be 17.88% and occurred at ~5 seconds after turning off the stimulation (Supplementary Fig. S4a-b). These results indicated that the TUT platform is capable of inducing transient bioeffects in a controllable manner and also enables imaging of these transient changes with high-speed and high-resolution optical microscopy techniques. This may be beneficial for studies that need only transient alternation of the membrane permeability to all the plated cells, which is not easily achievable with the conventional *in vitro* LIPUS methods.

Conclusions

In conclusion, we have developed a transparent LIPUS platform that allows high-throughput stimulation of cells plated directly on the biocompatible transparent ultrasound transducer (TUT) surface. TUTs were fabricated in a compact size of 3 mm × 3 mm × 2 mm and with a high light transmittance for easy integration with conventional optical microscopy setups. This allowed for simultaneous high-resolution imaging of live cell calcium fluorescence signaling using confocal laser scanning microscopy during mechanical stimulation. Quantitative single-cell fluorescence analysis further confirmed that the proposed TUT platform enables high-throughput and uniform stimulation of all plated cells. Cell stimulation experiments with varying acoustic stimulation parameters (duty cycle and pulse amplitude) revealed optimal LIPUS conditions for generating both mechanical (<1 °C temperature change) and thermal (>1 °C) bioeffects. The presented TUT platform has potential applications in studying mechanical stimulation of various types of biological cells and tissue and elucidate underlying mechanotransduction signalling pathways.

Materials and Methods

Ultrasound transducer fabrication and well plate preparation

A 250 μm thick 36˚ Y-cut $LiNbO_3$ (Precision Micro-Optics Inc., Burlington, MA) wafer was coated on both sides with a layer of 140 nm thick indium tin oxide (ITO) using electron-beam evaporation technique (OPCO Laboratory, Inc, Fitchburg, MA). $LiNbO_3$ was used as the active piezoelectric material due to its excellent piezoelectric and high optical transmission properties (31). The resulting ITO electrode had a sheet resistance of 10 Ω/square with a high light transmission rate (> 80%) across a broad wavelength range between 450 nm and 1500 nm. The transducer size was kept at 3 mm × 3 mm so it can be fit inside different standard diameters of well plates (range from 5.4 mm to 34.8 mm). The fabrication process was similar to our previously reported work (32). To maintain the light transparency, we used a colorless epoxy (Epotek-301, Epoxy Technologies Inc., Billerica, MA) as the backing layer. The transducer was housed inside a 1.5 mm height square brass tube. Such a compact size helped to maintain a reasonable

working distance for high-resolution microscopy imaging. The front electrode of the TUT was connected with the brass housing using a silver conductive epoxy (E-solder 3022, Von Roll Isola Inc., New Haven, CT). As the last step, a 500 µm thick micro glass slide was used to cover the back side of the TUT to flatten the epoxy and reduce possible light aberration. For an on-chip LIPUS, the TUT was adhered on the glass bottom of a 24-well plate using a thin layer of polydimethylsiloxane (PDMS) and cured at 60 °C for 2 hours. We then deposited a 2 µm thick Parylene C coating on the TUT and the well plates to improve the biocompatibility.

Hydrophone pressure field measurement

All the hydrophone measurements were conducted inside a tank filled with deionized (DI) water. A function generator produced a burst-mode sinusoidal waveform at a pulse repetition rate of 500 Hz at its resonant frequency (13 MHz). The Vpp of the sinusoidal wave was set to be 5 Volts at high impedance terminal and then amplified with a 20 dB gain using a power amplifier (Amplifier Research Corp., Souderton, PA). The absolute pressure output of TUTs was measured using a calibrated hydrophone (HGL0085, Onda, Sunnyvale, CA) with 85 µm aperture size and 0.25–40 MHz bandwidth. The hydrophone was scanned by a three-axis stage (NRT-1000, Thorlabs Inc., Newton, NJ) to generate the 3D pressure field in both near field (1 mm) and far field (natural focus at 20 mm) regions of the transducer. The scanning step size was set to 100 µm. The received voltage at the hydrophone was amplified by a preamplifier with 20 dB voltage gain and then captured using a data acquisition system (Razormax 16, GaGe, Lockport, IL) with 1 Giga sample per second sampling rate and 16 bits of resolution. The received voltage was then converted to absolute acoustic pressure by the company-supplied calibration chart. Ultrasound intensity parameters – I_{SPPA}, I_{SPTA}, MI – were then calculated using the methods described in (33).

Cell plating and calcium fluorescence imaging

After stabilized on a glass bottom 24 well plate, TUTs were treated with air plasma (800 mTorr, 30 W) for 2 minutes and were then coated with hexamethyldisilazane (Sigma, St. Louis, MO) for 8 min. Afterward, 50 µg/mL fibronectin solution (Thermo Fisher Scientific, Waltham, MA) was applied on the TUT surface for 30 min (34). 5637 bladder cancer cells (American Type Culture Collection, Manassas, VA, USA), maintained in RPMI 1640 Medium supplemented with 10% fetal bovine serum and 0.1% Gentamicin and cultured at 37 °C in a humidified incubator (5% CO_2 and 95% air), were seeded on the fibronectin-coated TUT. Cells were plated on the fibronectin-coated TUT with a density of 100,000 cells/cm² for 90 min, after which 750 mL culture media was added to each well and cultured overnight. To monitor the intracellular calcium level, 5637 cells were stained with 2 mM live cell calcium indicator Fluo-4, AM (Thermo Fisher Scientific, Waltham, MA), supplemented with 0.02% Pluronic F-127 (Thermo Fisher Scientific, Waltham, MA) and 1 mM probenecid (Sigma, St. Louis, MO) for 30 min at 37 °C per manufacturer's instruction. The cells were then washed with medium (no phenol red) and incubated for 30 min before imaging. The live cell calcium level was monitored by a Leica TCS SP8 confocal laser scanning microscope with an enclosure system (OKOlab, Italy) for temperature, humidity, and gas control for live cell experiments. The calcium indicator was excited with a 488 nm solid-state laser and the fluorescence signal was collected with a 10× air coupled objective lens at 1 frame per second.

LIPUS stimulation of cells

A pulsed waveform with desired peak to peak amplitude from the function generator was firstly amplified by a power amplifier (Amplifier Research Corp., Souderton, PA) with 20 dB gain before sending to the TUT. Each stimulation session was set to 110 seconds, which consisted of 10 seconds of baseline reading, 30 seconds of stimulation time (unless otherwise specified), and 70 seconds of post stimulation monitoring (unless otherwise specified). The imaging system continued to acquire both calcium fluorescence images and bright field images every 1 second (unless otherwise specified) during each imaging session of 110 seconds. The stimulation parameters were PRF – 500 Hz, fundamental frequency (FF) – 13 MHz, and desired duty cycle.

Single-cell analysis and statistical test

The fluorescent images of plated cells acquired using the confocal microscopy was post-processed in MATLAB (MathWorks, Natick, MA) to calculate the normalized calcium fluorescence change of each cell. First image segmentation masks were created by binarizing the first frame of each imaging session. From the binary mask, cell locations were then determined, and individual cell fluorescence was calculated by multiplying the logical mask by the true intensity raw image.

In order to determine the relative fluorescence change for each cell, baseline intensities were first calculated by averaging the cell intensities across all the frames acquired before the stimulation. These baselines were used to calculate the relative fluorescence value (ΔF/F) for each cell across all frames acquired during the stimulation and post-stimulation periods. Each cell's relative intensity change was plotted as a spectrogram, with elapsed time represented on the X axis and each cell represented on the Y axis. Furthermore, a line graph plots the averaged single-cell calcium responses versus time, with a shaded region depicting the standard deviation of fluorescence.

Two-sample t test was used to compare the effects of ultrasound stimulation and changing stimulation parameters. Statistical significance was determined by $p < 0.05$. Three asterisks indicating a p value less than 0.001.

Temperature measurement

The TUT surface temperature change was measured by a K-type point thermometer (T3000FC, Fluke Corporation, Everett, WA, USA) with 0.1 degree C precision and 4 samples per second temperature sampling rate. The temperature measurement procedures were conducted in a warm room to provide a consistent environment temperature and humidity. The TUT was placed in the well plate and the thermocouple was directly touching the transducer's surface measuring the real time temperature change while TUT was excited with different stimulation parameters. During the measurements, the TUT and the thermocouple were both submerged inside the deionized water to reduce possible electromagnetic field effect.

Finite element analysis modelling

COMSOL Multiphysics 5.6 (COMSOL Inc., Burlington, MA, USA) simulations was used to study possible mechanical vibrations of 3 mm × 3 mm TUT fabricated using a 36° rotated Y-cut transparent $LiNbO_3$ piezoelectric material. The boundaries of

the TUT were fixed from all sides to mimic the $LiNbO_3$ that was covered by the transparent epoxy. The simulation model was submerged inside the water. A 36° rotated Y-cut $LiNbO^3$ was modified from the predefined $LiNbO_3$ material property in COMSOL with a rotated system based on Euler angles (0°, 36.26°, 0°). Exciting this crystal that coated with electrodes along the thickness mode with 30 Vpp (3 Vpp and 20 dB gain), the effective electromechanical coupling factor is highest in quasi-longitudinal direction whereas the effective electromechanical coupling factors contributing to pure shear and quasi-shear mode vibration are theoretically close to zero (35, 36). Due to this unique property, the resulting mechanical vibration for the TUT is dominated in quasi-longitudinal mode along the direction of the propagation of the wave (Supplementary Video S1). These simulation results showed that the vibrational amplitude of hundreds of picometers, and the maximum displacement occurs at the center. Considering the speed of vibration was quite fast, the cells directly plated on top of the transducer therefore exerted the similar vibration modes, leading to uniform mechanical stimulation.

Acknowledgement

This research was funded by NIH-NIBIB R00EB017729-04 (SRK), the Penn State Cancer Institute—Highmark seed grant (SRK), NSF Biophotonics Program 1802947 (PKW) and Grace Woodward grants (SRK). We acknowledge Eugene Gerber for his kind support in the machining of parts and help with transducer design. We also thank Christopher Cheng with his help in Parylene coating.

Author Contributions

Conceptualization H.C., and S.-R.K.; implementation H.C., N.Z., P.K.W and S.-R.K.; software, H.C., N.Z., and R.B.; investigation, P.B., P.K.W., and S.-R.K.; biological resources, N.Z., and P.K.W; data curation, H.C., J.L., and R.B.; writing: original-draft preparation, H.C.; experiment design, H.C., and S.-R.K.; hardware, H.C., J.L., and M.O.; project administration, S.-R.K.; funding acquisition, P.K.W. and S.-R.K.

Conflicts of Interest

Authors declare no conflicts of interests.

References

1. Jiang X, Savchenko O, Li Y, Qi S, Yang T, Zhang W, et al. A Review of Low-Intensity Pulsed Ultrasound for Therapeutic Applications. IEEE Trans Biomed Eng. 2019;66(10):2704-18.
2. Lin G, Reed-Maldonado AB, Lin M, Xin Z, Lue TF. Effects and Mechanisms of Low-Intensity Pulsed Ultrasound for Chronic Prostatitis and Chronic Pelvic Pain Syndrome. Int J Mol Sci. 2016;17(7).
3. Nakamura T, Fujihara S, Yamamoto-Nagata K, Katsura T, Inubushi T, Tanaka E. Low-intensity pulsed ultrasound reduces the inflammatory activity of synovitis. Ann Biomed Eng. 2011;39(12):2964-71.
4. Hadjiargyrou M, McLeod K, Ryaby JP, Rubin C. Enhancement of fracture healing by low intensity ultrasound. Clin Orthop Relat Res. 1998(355 Suppl):S216-29.
5. Katiyar A, Osborn J, DasBanerjee M, Zhang LG, Sarkar K, Sarker KP. Inhibition of Human Breast Cancer Cell Proliferation by Low-Intensity Ultrasound Stimulation. J Ultrasound Med. 2020;39(10):2043-52.
6. Jang KW, Ding L, Seol D, Lim TH, Buckwalter JA, Martin JA. Low-intensity pulsed ultrasound promotes chondrogenic progenitor cell migration via focal adhesion kinase pathway. Ultrasound Med Biol. 2014;40(6):1177-86.
7. Yoon S, Kim MG, Chiu CT, Hwang JY, Kim HH, Wang Y, et al. Direct and sustained intracellular delivery of exogenous molecules using acoustic-transfection with high frequency ultrasound. Sci Rep. 2016;6:20477.
8. Fan Z, Liu H, Mayer M, Deng CX. Spatiotemporally controlled single cell sonoporation. Proc Natl Acad Sci U S A. 2012;109(41):16486-91.
9. Humphrey JD, Dufresne ER, Schwartz MA. Mechanotransduction and extracellular matrix homeostasis. Nat Rev Mol Cell Biol. 2014;15(12):802-12.
10. Hong X, Annamalai RT, Kemerer TS, Deng CX, Stegemann JP. Multimode ultrasound viscoelastography for three-dimensional interrogation of microscale mechanical properties in heterogeneous biomaterials. Biomaterials. 2018;178:11-22.
11. Alvarenga EC, Rodrigues R, Caricati-Neto A, Silva-Filho FC, Paredes-Gamero EJ, Ferreira AT. Low-intensity pulsed ultrasound-dependent osteoblast proliferation occurs by via activation of the P2Y receptor: role of the P2Y1 receptor. Bone. 2010;46(2):355-62.
12. Padilla F, Puts R, Vico L, Raum K. Stimulation of bone repair with ultrasound: a review of the possible mechanic effects. Ultrasonics. 2014;54(5):1125-45.
13. Zhou Y, Shi J, Cui J, Deng CX. Effects of extracellular calcium on cell membrane resealing in sonoporation. J Control Release. 2008;126(1):34-43.
14. Weitz AC, Lee NS, Yoon CW, Bonyad A, Goo KS, Kim S, et al. Functional Assay of Cancer Cell Invasion Potential Based on Mechanotransduction of Focused Ultrasound. Front Oncol. 2017;7:161.
15. Lacroix JJ, Ozkan AD. Multiplexing Focused Ultrasound Stimulation with Fluorescence Microscopy. J Vis Exp. 2019(143).
16. Li J, Zhang Q, Ren C, Wu X, Zhang Y, Bai X, et al. Low-Intensity Pulsed Ultrasound Prevents the Oxidative Stress Induced Endothelial-Mesenchymal Transition in Human Aortic Endothelial Cells. Cell Physiol Biochem. 2018;45(4):1350-65.
17. Hu B, Zhang Y, Zhou J, Li J, Deng F, Wang Z, et al. Low-intensity pulsed ultrasound stimulation facilitates osteogenic differentiation of human periodontal ligament cells. PLoS One. 2014;9(4):e95168.
18. Sena K, Angle SR, Kanaji A, Aher C, Karwo DG, Sumner DR, et al. Low-intensity pulsed ultrasound (LIPUS) and cell-to-cell communication in bone marrow stromal cells. Ultrasonics. 2011;51(5):639-44.
19. Dangi A, Agrawal S, Kothapalli SR. Lithium niobate-based transparent ultrasound transducers for photoacoustic imaging. Opt Lett. 2019;44(21):5326-9.
20. Harrison A, Alt V. Low-intensity pulsed ultrasound (LIPUS) for stimulation of bone healing - A narrative review. Injury. 2021;52 Suppl 2:S91-S6.
21. Ding X, Lin SC, Lapsley MI, Li S, Guo X, Chan CY, et al. Standing surface acoustic wave (SSAW) based multichannel cell sorting. Lab Chip. 2012;12(21):4228-31.
22. Nelson TR, Fowlkes JB, Abramowicz JS, Church CC. Ultrasound biosafety considerations for the practicing sonographer and sonologist. J Ultrasound Med. 2009;28(2):139-50.

23. Miyasaka M, Nakata H, Hao J, Kim Y, Kasugai S, Kuroda S. Low-Intensity Pulsed Ultrasound Stimulation Enhances Heat-Shock Protein 90 and Mineralized Nodule Formation in Mouse Calvaria-Derived Osteoblasts. Tissue Engineering Part a. 2015;21(23-24):2829-39.
24. Claes L, Willie B. The enhancement of bone regeneration by ultrasound. Prog Biophys Mol Biol. 2007;93(1-3):384-98.
25. Chen J, Jiang J, Wang W, Qin J, Chen W, Wang Y. Low intensity pulsed ultrasound promotes the migration of bone marrow- derived mesenchymal stem cells via activating FAK-ERK1/2 signalling pathway. Artif Cells Nanomed Biotechnol. 2019;47(1):3603-13.
26. Kennedy A. Fetal ultrasound. Curr Probl Diagn Radiol. 2000;29(4):109-40.
27. Schibber EF, Mittelstein DR, Gharib M, Shapiro MG, Lee PP, Ortiz M. A dynamical model of oncotripsy by mechanical cell fatigue: selective cancer cell ablation by low-intensity pulsed ultrasound. Proc Math Phys Eng Sci. 2020;476(2236):20190692.
28. Fang HY, Tsai KC, Cheng WH, Shieh MJ, Lou PJ, Lin WL, et al. The effects of power on-off durations of pulsed ultrasound on the destruction of cancer cells. Int J Hyperthermia. 2007;23(4):371-80.
29. Chang WH, Sun JS, Chang SP, Lin JC. Study of thermal effects of ultrasound stimulation on fracture healing. Bioelectromagnetics. 2002;23(4):256-63.
30. Xue H, Zheng J, Cui Z, Bai X, Li G, Zhang C, et al. Low-intensity pulsed ultrasound accelerates tooth movement via activation of the BMP-2 signaling pathway. PLoS One. 2013;8(7):e68926.
31. Zhou Q, Lam KH, Zheng H, Qiu W, Shung KK. Piezoelectric single crystals for ultrasonic transducers in biomedical applications. Prog Mater Sci. 2014;66:87-111.
32. Chen H, Agrawal S, Dangi A, Wible C, Osman M, Abune L, et al. Optical-Resolution Photoacoustic Microscopy Using Transparent Ultrasound Transducer. Sensors (Basel). 2019;19(24).
33. Agrawal S, Johnstonbaugh K, Clark JY, Raman JD, Wang X, Kothapalli SR. Design, Development, and Multi-Characterization of an Integrated Clinical Transrectal Ultrasound and Photoacoustic Device for Human Prostate Imaging. Diagnostics (Basel). 2020;10(8).
34. Zhu N, Kwong H, Bao Y, Chen T. Chiral Orientation of Skeletal Muscle Cells Requires Rigid Substrate. Micromachines. 2017;8(6).
35. Ka-Kha W. Properties of Lithium Niobate: London : INSPEC/Institution of Electrical Engineers; 2002.
36. Kadota M, Ogami T, Kimura T, Daimon K. Tunable filters using wideband elastic resonators. IEEE Trans Ultrason Ferroelectr Freq Control. 2013;60(10):2129-36.

